

# A semi-automated analysis pipeline for reproducible SWI analysis of multiple sclerosis pathology

M. G. Dwyer<sup>1</sup>, N. Bergsland<sup>2</sup>, C. Schirda<sup>2</sup>, M. Heininen-Brown<sup>3</sup>, E. Carl<sup>1</sup>, D. Wack<sup>1</sup>, G. U. Poloni<sup>1</sup>, and R. Zivadinov<sup>4</sup>

<sup>1</sup>Buffalo Neuroimaging Analysis Center, <sup>2</sup>University at Buffalo, Buffalo Neuroimaging Analysis Center, Buffalo, NY, United States, <sup>3</sup>University at Buffalo, Buffalo Neuroimaging Analysis Center, Buffalo, NY, <sup>4</sup>Neurology, Buffalo Neuroimaging Analysis Center, Buffalo, NY, United States

## BACKGROUND

Susceptibility-weighted imaging (SWI) has been shown to provide a very sensitive means for detecting changes in brain iron content in patients with multiple sclerosis (MS). However, its direct interpretation can be difficult due to noise, high-pass filter effects, and structural variability. In addition, the relationship between SWI and other established MRI indicators of disease progression is not well understood. To address these issues, we propose a method for standardized and reproducible semi-automated quantification of SWI-visible iron content and its relationship to other MRI measures in specific areas of the brain.

## METHODS

**MRI acquisition and reconstruction:** For each patient, SWI was acquired on a GE 3.0 Tesla scanner. In addition, MTR, perfusion, and conventional FLAIR and T1-SE images were acquired. SWI phase and magnitude images were reconstructed from raw data and the phase image was high-pass filtered using a 64x48 Hanning window. Correction for geometric field-induced distortions was carried out via FSL's FNIRT utility. Images were composited as described in (Haacke et al., 2009).

**Lesion analysis:** T2 lesions, T1 black holes, SWI magnitude-visible lesions, and SWI phase-visible lesions were identified and delineated using a previously described semi-automated edge contouring technique. Phase-visible lesions were further subdivided into nodular, ring-shaped, and scattered categories. All lesion masks were co-registered onto an up-sampled subject-specific FLAIR space, at which point spatial overlap maps were calculated. These were in turn used to calculate mean magnitude and phase values for each lesion type and each intersection of lesion types.

**Regional analysis:** The high-resolution T1-weighted image was then segmented and into various tissue classes and regions. Sub-cortical gray matter structures were segmented using a combination of semi-automated edge-contouring and FMRIB's Integrated Registration and Segmentation Tool (FIRST); specifically, thalamus, caudate, putamen, globus pallidus, hippocampus, amygdala, and nucleus accumbens were identified via FIRST, and the red nucleus, pulvinar nucleus of the thalamus, and substantia nigra were identified semi-automatically. In addition, the image was deskulled and segmented into tissue-specific compartments via FMRIB's automated segmentation tool (FAST). Lesion masks were also used to distinguish between whole brain tissue compartments and normal-appearing tissue compartments. As with the lesion measurements, mean non-vein phase and magnitude values were calculated for each sub-cortical region and each tissue compartment.

**MTR and perfusion:** MTR and perfusion CBV, CBF, and MTT mapping were performed according to well-established techniques. These maps were then overlaid with the SWI data via co-registration into the subject-specific FLAIR space.

## RESULTS

The program was assembled as an integrated pipeline, and was successfully run on a large group of subject scans (200). Program results were very reproducible (average  $r=0.96$  on scan-rescan) and provided for a better understanding of the differences in iron content between different disease groups.

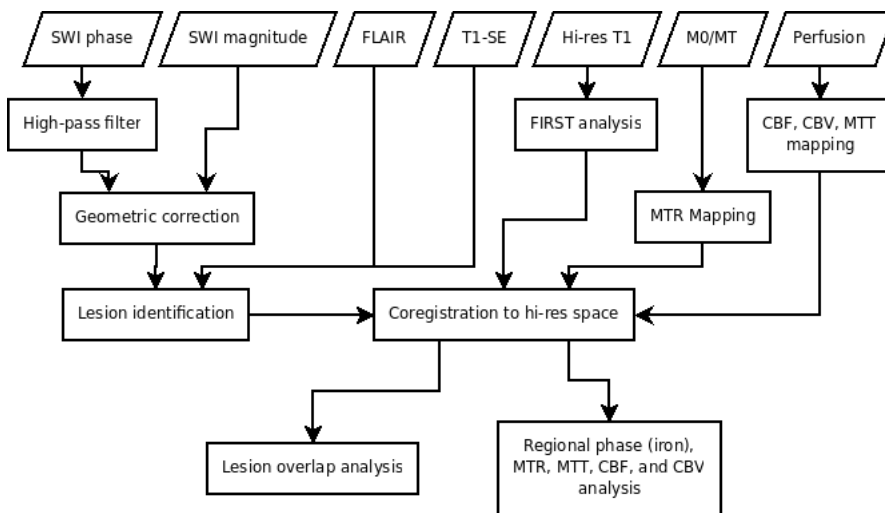


Figure 2: Flowchart of SWI processing steps

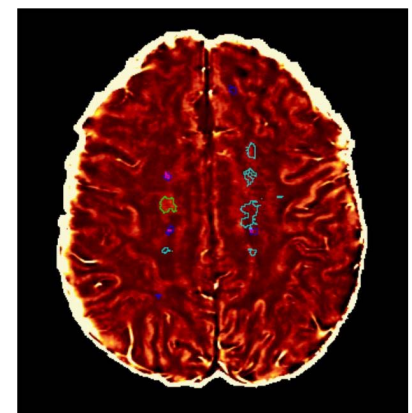


Figure 1: Lesion categories overlaid on SWI phase image.